Computational Water, Energy, and Environmental Engineering, 2026, 15(3), 73-96
https://www.scirp.org/journal/cweee
ISSN Online: 2168-1570
ISSN Print: 2168-1562

Development of a Steam Turbine Using the Quasi-3D Inverse Design Method

Ayodele T. Oyeniran[1,2], Ayomide E. Oyedare[1], Olamilekan G. Agbedun[1], Daniel S. Taiwo[1], Samson K. Fasogbon[3,4,5], Opeyemi B. Daniyan[6]*, Abraham A. Asere[7]

[1]Mechanical Engineering Department, Obafemi Awolowo University, Ile-Ife, Nigeria
[2]Aerospace Engineering Department, Obafemi Awolowo University, Ile-Ife, Nigeria
[3]Department of Mechanical Engineering, University of Ibadan, Ibadan, Nigeria
[4]Centre for Petroleum, Energy Economics & Law, University of Ibadan, Ibadan, Nigeria
[5]Department of Biomedical Engineering, University of Ibadan, Ibadan, Nigeria
[6]Department of Computer Science and Cybersecurity, Obafemi Awolowo University, Ile-Ife, Nigeria
[7]Department of Automotive Engineering, Elizade University, Ilara Mokin, Nigeria
Email: *odaniyan@oauife.edu.ng

How to cite this paper: Oyeniran, A.T., Oyedare, A.E., Agbedun, O.G., Taiwo, D.S., Fasogbon, S.K., Daniyan, O.B. and Asere, A.A. (2026) Development of a Steam Turbine Using the Quasi-3D Inverse Design Method. *Computational Water, Energy, and Environmental Engineering*, **15**, 73-96.
https://doi.org/10.4236/cweee.2026.153005

Received: June 12, 2026
Accepted: July 25, 2026
Published: July 28, 2026

Abstract

The growing demand for sustainable and efficient energy conversion has highlighted the limitations of conventional forward design approaches in steam turbine development. These geometry-driven methods often rely on iterative optimization and fail to capture complex 3D flow phenomena such as secondary flows, vortex formation, and entropy gradients. This study applies the Inverse Design Method (IDM) to the design of a single-stage axial flow steam turbine, providing a flow-driven alternative that directly prescribes aerodynamic performance. on a 2D A quasi-3D IDM framework was derived from the compressible Navier-Stokes equations, incorporating entropy effects through the streamfunction-vorticity formulation. The governing equations were solved numerically meridional grid in MATLAB. Thermodynamic closure employed real steam properties from the IAPWS-IF97 property table. The resulting blade angles, wrap-angle distributions, and hybrid Zangeneh loading (fore-loaded hub, aft-loaded shroud) were implemented in the CFturbo IDM solver to generate the three-dimensional blade geometries for the inlet stator, rotor, and outlet stator, which were subsequently validated through CFD simulations in ANSYS CFX using real steam properties. CFD results showed close quantitative agreement with MATLAB and CFturbo predictions: blade angle and pressure ratio deviations were <5% and stage efficiency was consistent with literature values (isentropic efficiency ~0.707). Minimal secondary flow phenomena were observed, with mesh-independence results (<5% change key metrics) and limited turbulence model sensitivity (SST k-ω baseline). Finally, a scaled prototype turbine was fabricated by fused deposition modeling (FDM) to demonstrate practical feasibility. The study establishes IDM as a rigorous and practical methodology for steam turbine blade design, bridging theoretical derivation with industrial application.

Keywords

Inverse Design Method, Steam Turbine, Quasi-3D, CFD, CFturbo, MATLAB, ANSYS CFX

1. Introduction

Energy is widely recognized as the cornerstone of modern human activity and development, often defined as "*the capacity to perform work*". This foundational concept highlights the crucial role of energy production in sustaining industrial processes, transportation, power generation, and technological advancements [1]. As global energy demand continues to rise, achieving reliable, efficient, and sustainable energy conversion has become a central engineering challenge. Among the viable solutions to the energy generation crisis, turbomachinery, encompassing steam and gas turbines, pumps, and compressors, plays a significant role in this pursuit. These machines are central to power generation, marine propulsion, and industrial energy systems, including applications in steam power plants, gas turbine stations, nuclear power plants, ships, and submarines [2] [3].

The steam turbine, which is the focus of this study, has relevance that stems from its ability to convert thermal and fluid energy to mechanical work efficiently while offering high power density and, when coupled with renewable or low-carbon sources, has minimal environmental impact [4]. Their performance depends on the coordinated operation of components such as the casing, rotor, blades, nozzles, bearings, seals, and steam flow systems. Among these, blade geometry plays a critical role in determining aerodynamic efficiency, pressure distribution, and loss mechanisms within the turbine stages. The underlying engineering principle behind the operation of steam turbines is the generation of mechanical work from the expansion of high-temperature and high-pressure steam within an assembly of nozzles and aerodynamically curved blades. This is achieved by the transfer of energy and momentum from fast-moving steam to the blades of the turbine [5] [6].

Historically, the design of turbomachinery blades relied on the conventional forward (direct) design methods, where the blade geometry is prescribed and iteratively optimized using empirical formulas and correlations, analytical models, and computational fluid dynamics (CFD) analyses (Denton, 1999; Giuffre & Pini, 2020). Although widely adopted, this method is time-intensive, computationally demanding, and often limited in its ability to capture and predict complex three-dimensional flow phenomena such as secondary flows, vortex formation, entropy gradients, and boundary-layer separation, which can contribute to efficiency losses of up to 4% - 6% in highly loaded turbine stages [7] [8].

To address these limitations, the Inverse Design Method (IDM) emerged in the late 20th century, offering a flow-driven approach to blade generation. Unlike the forward design method, IDM starts from the desired flow and aerodynamic performance metrics, such as blade loading, velocity distribution, and pressure profiles, and derives the corresponding blade surface geometry by solving the governing flow equations iteratively until the flow streamlines are tangent to the blade surface [9] [10].

The Inverse Design Methodology derives its roots from World War II, when the flow-oriented design approach was first applied to rocket propulsion systems. The IDM principles were developed primarily for hydraulic pumps and compressors under the 2-D, incompressible potential-flow formulations. Wu's formulation in 1952 established the basis for introducing relative stream surfaces, which significantly influenced the subsequent research and the development of the quasi-3D IDM approaches [11].

Further research in the late 20th century by Hawthorne, Tan, Borges, and later, Zangeneh advanced the methodology into 3-D forms, incorporating mean swirl distribution, periodic flow, and compressibility corrections [12] [13] (Zangeneh & Hawthorne, 1990; Boselli, 2016). Further developments incorporated pressure-specified formulations and Navier-Stokes-based viscous flow models, improving predictive accuracy and enabling applications to compressors, turbines, and blade cascades [14]-[16]. Comparative studies have demonstrated that inverse-designed blades can improve turbine stage efficiency by approximately 2% - 4% and reduce secondary flow losses by up to 30% in highly loaded stages [13] [14] (Hosseini *et al.*, 2023; Zhou *et al.*, 2022). The IDM enhances design flexibility, enabling engineers to suppress adverse flow phenomena that would be difficult to predict with conventional methods [14] [15].

Recent advancements in CFD, turbulence modelling, and specialized turbomachinery software such as CFturbo and ANSYS have enhanced the implementation and validation of IDM-based designs. Techniques such as Reynolds-averaged Navier-Stokes (RANS) and Large Eddy Simulation (LES) enable more accurate prediction of complex flow structures and loss mechanisms (Smith, 2020). However, many existing IDM implementations remain computationally intensive and require substantial computational resources.

Therefore, the reviewed literature establishes IDM as a robust and efficient alternative to conventional blade design methods, offering improved aerodynamic control and performance optimization. Nevertheless, there remains a need for simplified, validated, and resource-conscious IDM workflows suitable for preliminary steam turbine blade design. Addressing this gap forms the basis of the present study, which integrates mathematical modelling, CFD validation, and practical prototyping to develop an efficient IDM-based design framework for axial steam turbines.

This study aims to highlight the mathematical rigor of IDM, its workflow in industrial software, and its relevance for high-efficiency energy conversion in modern turbomachinery. The methodology adopted involves the application of the inverse design method in steam turbine blade design, leveraging the CFturbo IDM flow solver combined with mathematical preprocessing in MATLAB and CFD validation using ANSYS.

2. Materials and Methods

The Inverse Design Method (IDM) adopts a classical fluid mechanics framework derived from the compressible Navier-Stokes equations. This formulation integrates a physically intuitive torque-momentum relationship with an industrial turbomachinery design workflow to produce a flow-driven blade generation process.

The research methodology comprises four interconnected stages (**Figure 1**). First, the governing equations for compressible axial flow are formulated from the Navier-Stokes and streamfunction-vorticity equations, forming the foundation of the fluid mechanics model. Second, the quasi-3D streamfunction-vorticity equations are solved numerically using MATLAB to determine the blade wrap angle and inlet/outlet flow angles. Third, these computed flow parameters are implemented within CFturbo's IDM module to generate a three-dimensional blade geometry that satisfies the prescribed aerodynamic parameters and the flow tangency condition. Fourth, computational fluid dynamics (CFD) validation is conducted in ANSYS CFX with real steam properties from the IAPWS table, incorporating mesh independence studies and turbulence model sensitivity studies. A scaled prototype is fabricated via FDM as a final feasibility demonstration.

The classical Navier-Stokes equation, coupled with the streamfunction-vorticity derivation, provides the standard quasi-3D inverse design PDE. This multifaceted approach ensures that the theoretical background of the inverse design methodology aligns with the practical design and validation, thereby fulfilling the research objectives of mathematical rigor and application-driven design.

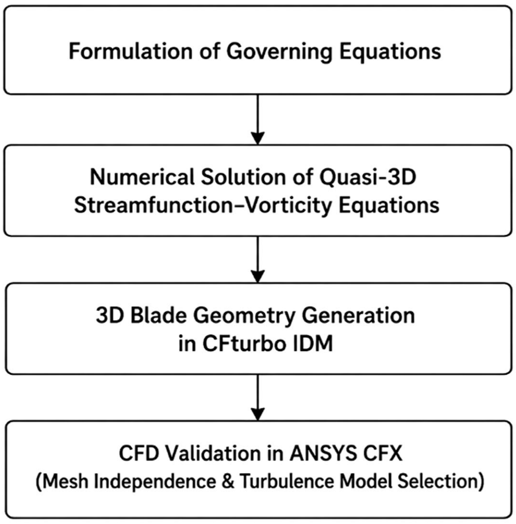

Figure 1. Flowchart of the quasi-3D IDM for steam turbine blade design.

2.1. Mathematical Framework and Flow Assumptions

The inverse design of an axial flow steam turbine requires a rigorous mathematical framework based on fundamental fluid dynamics principles. The governing equations are derived from the compressible Navier-Stokes equations in the cylindrical coordinate system.

The flow assumptions valid for the compressible axial flow steam turbine are described below:

- Steady flow,
- Compressible flow (properties for steam are obtained from IAPWS tables),
- Adiabatic, inviscid flow (viscous effects confined to boundary layers),
- Axisymmetric flow, and
- Flow predominantly along the meridional streamline (azimuthal/tangential variables are negligible).

2.1.1. Continuity Equation

The general mass conservation equation in cylindrical coordinates is described by:

$$\frac{\partial \rho}{\partial t}+\nabla\cdot\left(\rho u\right)=0 \tag{2.1a}$$

$$\frac{\partial \rho}{\partial t}+\frac{1}{r}\frac{\partial\left(r\rho u_r\right)}{\partial r}+\frac{1}{r}\frac{\partial\left(\rho u_\theta\right)}{\partial \theta}+\frac{\partial\left(\rho u_z\right)}{\partial z}=0 \tag{2.1b}$$

Under the flow assumptions stated earlier, the continuity equation for the steady, axisymmetric compressible flow becomes

$$\frac{1}{r}\frac{\partial\left(r\rho u_r\right)}{\partial r}+\frac{\partial\left(\rho u_z\right)}{\partial z}=0 \tag{2.2}$$

2.1.2. Momentum Equation

The conservation of momentum equation is obtained by applying Newton's second law of motion to the fluid element, which is the control volume around the blade cascade.

$$\sum F=m\frac{\mathrm{d}V}{\mathrm{d}t} \tag{2.3}$$

The general momentum equation in the cylindrical coordinate system is given by:

$$\rho\left(\frac{\partial u}{\partial t}+\left(u\cdot\nabla\right)u\right)=-\nabla p+\mu\nabla^2 u+F \tag{2.4a}$$

The axial projection of the general momentum equation gives the following:

$$\rho\left(\frac{\partial u_z}{\partial t}+u_r\frac{\partial u_z}{\partial r}+\frac{1}{r}u_\theta\frac{\partial u_z}{\partial \theta}+u_z\frac{\partial u_z}{\partial z}\right)=-\frac{\partial p}{\partial z}+\nabla\cdot\tau_z+F_z \tag{2.4b}$$

Applying the steady, axisymmetric, and inviscid-outside-boundary-layer flow assumptions stated earlier, the momentum equation reduces to:

$$\rho\left(u_r\frac{\partial u_z}{\partial r}+u_z\frac{\partial u_z}{\partial z}\right)=-\frac{\partial p}{\partial z} \tag{2.5}$$

2.1.3. Streamfunction-Vorticity Formulation

The Stokes streamfunction, originally defined for incompressible axisymmetric flow, is extended here to compressible flow through the introduction of a density-weighted streamfunction $\Psi(r,z)$ that identically satisfies the compressible continuity equation (Equation (2.2)).

The potential flow assumes inviscid and irrotational flow, in which the velocity vector can be expressed as the gradient of a scalar function, called the velocity potential ϕ. Conversely, the term "vorticity", ω, is a measure of the local rotation or spin of a fluid element, which is the curl of the velocity vector. They can be expressed mathematically as

$$v = \nabla \phi \tag{2.6}$$

$$\omega = \nabla \times \underline{v} \tag{2.7}$$

The Stokes streamfunction ψ, which automatically satisfies the continuity equation, is given as:

$$\frac{1}{r}\frac{\partial}{\partial r}(ru_r) + \frac{\partial}{\partial z}(ru_z) = 0 \tag{2.8a}$$

$$\frac{\partial}{\partial r}\left(\frac{\partial \Psi}{\partial r}\right) + \frac{\partial}{\partial z}\left(-\frac{\partial \Psi}{\partial z}\right) = 0 \tag{2.8b}$$

In the steady-state, compressible axisymmetric flow, the continuity equations are expressed in Equation (2.2). To satisfy the continuity equation identically, a compressible streamfunction $\psi(r,z)$ is introduced.

$$\rho r u_r = -\frac{\partial \Psi}{\partial z}, \quad \rho r u_z = \frac{\partial \Psi}{\partial r} \tag{2.9}$$

Contrary to the potential flow assumption of irrotational flow, the presence of blades introduces vorticity, or local rotation, to the flow. Introducing the compressible streamfunction into the circumferential vorticity equation in Equation (2.7) gives the governing elliptical PDE for the streamfunction.

$$\omega_\theta(r,z) = \frac{\partial}{\partial r}\left(\frac{1}{\rho r}\frac{\partial \Psi}{\partial r}\right) + \frac{\partial}{\partial z}\left(-\frac{1}{\rho r}\frac{\partial \Psi}{\partial z}\right) \tag{2.10}$$

The change in the tangential velocity across a blade cascade is a measure of the work done by or on the fluid as a result of the transfer or transport of momentum, which is described as the blade loading. This change in tangential velocity is directly related to the circulation Γ around the blade.

The source term is a function of the change in angular momentum. This is the governing equation that describes the quasi-3D inverse design method. In vector notation, the quasi-3D IDM governing equation can be expressed as

$$\nabla \cdot \left(\frac{1}{r\rho}\nabla \psi\right) = \omega_\theta = -\frac{\partial \Gamma}{\partial s} \tag{2.11}$$

The LHS of the equation represents the divergence of the mass flux, *i.e.*, the potential flow part, while the RHS represents the circulation around the blade (vorticity), which is a function of the blade loading from the Kutta-Joukowski theorem.

2.1.4. Radial Equilibrium with Entropy Effects

The radial equilibrium equation is derived by combining the Navier-Stokes momentum equation under the steady, axisymmetric, radial, and through-flow assumption with the fundamental thermodynamic relation. The steady-state, axisymmetric flow assumption for the turbine annulus reduces the radial component of the momentum equation to:

$$\rho\left(u_r\frac{\partial u_r}{\partial r}+u_z\frac{\partial u_r}{\partial z}-\frac{1}{r}u_\theta^2\right)=-\frac{\partial p}{\partial r} \tag{2.12a}$$

The equation represents the general radial momentum balance equation, accounting for the radial convective accelerations and the centrifugal force. For a thin annulus (through-flow assumption), the convective terms of the meridional acceleration u_r are relatively small compared to the centrifugal term, thus negligible. The radial momentum balance equation reduces to

$$\frac{\partial p}{\partial r}\approx\frac{\rho}{r}u_\theta^2 \tag{2.12b}$$

The fundamental thermodynamic relations describe the changes in the thermodynamic state functions of the system. The total derivative of the equation with respect to the radial coordinate is expressed as

$$\mathrm{d}h=T\mathrm{d}s+v\mathrm{d}p \tag{2.13a}$$

$$\frac{\mathrm{d}h}{\mathrm{d}r}=T\frac{\mathrm{d}s}{\mathrm{d}r}+v\frac{\mathrm{d}p}{\mathrm{d}r} \tag{2.13b}$$

Combining the fundamental thermodynamic relation with the radial momentum balance equations leads to the radial equilibrium equation with entropy effects as expressed below:

$$\frac{\mathrm{d}p}{\mathrm{d}r}=\frac{1}{v}\left(\frac{\mathrm{d}h}{\mathrm{d}r}-T\frac{\mathrm{d}s}{\mathrm{d}r}\right) \tag{2.13c}$$

$$\frac{\rho}{r}u_\theta^2=\frac{1}{v}\left(\frac{\mathrm{d}h}{\mathrm{d}r}-T\frac{\mathrm{d}s}{\mathrm{d}r}\right) \tag{2.13d}$$

For a thermodynamic system, the pressure is a state function; therefore, its differential must be exact. For some differentiable scalar function, $z=z(x,y)$, the exact differential form in the open domain, $D\subset R^2$, can be expressed mathematically as:

$$\mathrm{d}z=M(x,y)\mathrm{d}x+N(x,y)\mathrm{d}y \tag{2.14a}$$

The condition for exactness of the differential is that the mixed partial derivatives are equal. In the thermodynamics domain, it can be written as

$$\mathrm{d}p=\left(\frac{\mathrm{d}p}{\mathrm{d}\rho}\right)_s\mathrm{d}\rho+\left(\frac{\mathrm{d}p}{\mathrm{d}s}\right)_\rho\mathrm{d}s \tag{2.14b}$$

where $\left(\frac{\mathrm{d}p}{\mathrm{d}\rho}\right)_s$ is the square of the isentropic speed of sound, and $\left(\frac{\mathrm{d}p}{\mathrm{d}s}\right)_\rho$ is a thermodynamic coefficient.

$$\mathrm{d}p = a^2 \mathrm{d}\rho + \rho T \mathrm{d}s \tag{2.14c}$$

Taking the derivative of this equation above with respect to the radial coordinate and combining it with the radial equilibrium equation obtained earlier gives:

$$a^2 \frac{\mathrm{d}\rho}{\mathrm{d}r} + \rho T \frac{\mathrm{d}s}{\mathrm{d}r} = \frac{\rho}{r} u_\theta^2 \tag{2.14d}$$

The equation above is the compressible radial-equilibrium equation with entropy effects.

2.2. Numerical Solution in MATLAB

The quasi-3D IDM governing equation (Equation (2.11)) is solved numerically on a 2D computational grid spanning the meridional ξ and spanwise η directions. The grid comprises $(n_i, n_j) = (60, 20)$ streamwise and spanwise nodes, generated algebraically using linear interpolation between the hub and shroud endwall coordinates, with metric tensor components and Jacobian evaluated using central differences on interior nodes and one-sided differences at the boundaries.

The numerical procedure uses two nested loops on distinct unknowns:

- **Inner loop**: Solves the full 2D streamfunction field $\Psi(\xi, \eta)$ at fixed blade geometry via sparse finite-difference matrix $A\Psi = b$.
- **Outer loop**: Updates the 2D wrap-angle field $f(\xi, \eta)$ from the converged flow field via independent 1D trapezoidal integration along each of the 20 meridional streamlines.

2.2.1. Boundary Conditions

The Dirichlet and Neumann boundary conditions are applied at the inlet, outlet, hub, and shroud as follows:

- Inlet $(\xi = 0)$: Dirichlet condition $\psi = \dot{m} \cdot \frac{j-1}{n_j - 1}$, $j = 1, 2, 3, \cdots, n_j$
- Hub $(\eta = 0)$: $\psi = 0$
- Shroud $(\eta = 1)$: $\psi = \dot{m}$
- Outlet/Trailing edge $(\xi = 1)$: Neumann condition $\partial\Psi/\partial\xi = 0$

These conditions are enforced directly in the sparse matrix assembly. The compressible streamfunction is initialized with a linear spanwise distribution consistent with uniform mass flow.

2.2.2. Computation Algorithm and Prescribed Loading

The computation of the desired flow parameters is a multi-stage process as expressed in the flowchart below (**Figure 2**).

The computation of the desired flow parameters was carried out through a multi-stage iterative procedure involving the specification of the turbine design and operating conditions, definition of the meanline geometry, numerical solution of the governing equations, and convergence evaluation.

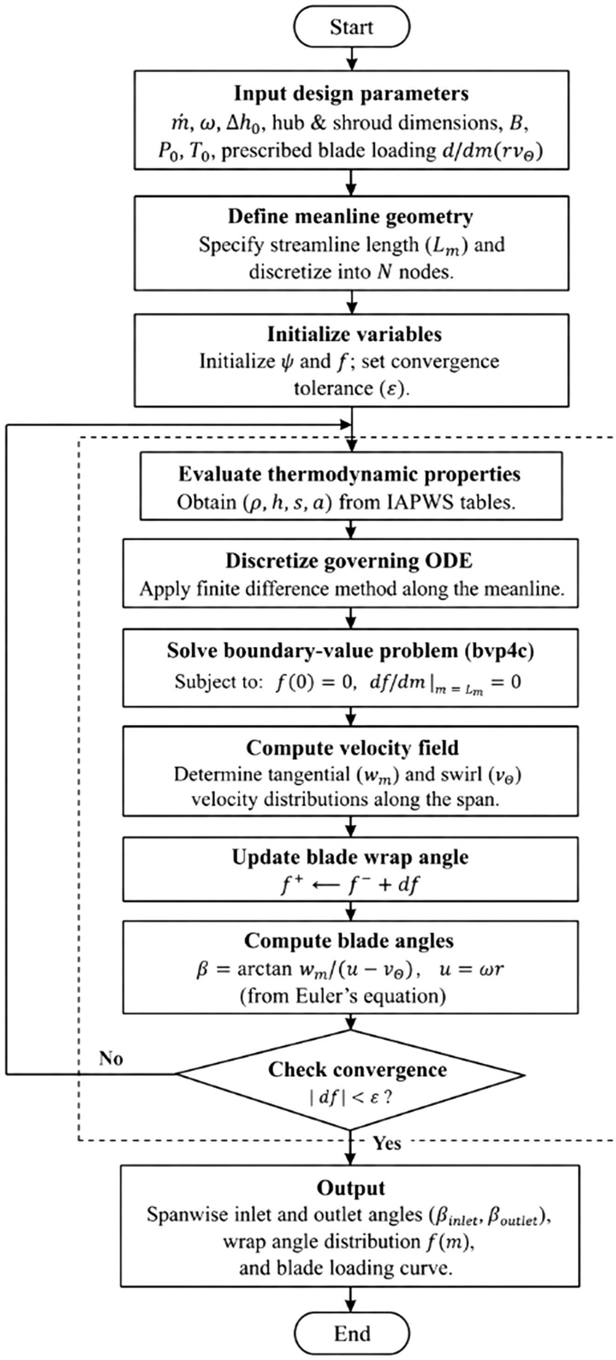

Figure 2. Computational algorithm flowchart.

The process begins with the input of the principal design parameters (**Table 1**), including the mass flow rate ($\dot{m}$), rotational speed (N), stage enthalpy drop (Δh_o), hub and shroud dimensions, number of blades (Z), inlet pressure and temperature (P_o, T_o), and the prescribed blade loading distribution.

The prescribed loading distribution is defined following the Zangeneh (1990) parameterization. The cumulative swirl shape function $G(\xi)$ is a monotone PCHIP (Piecewise Cubic Hermite Interpolating Polynomial) interpolant over the normalized meridional chord $\xi = (m - m_{LE})/L_{chord} \in [0,1]$, passing through the control points

$$\{(\xi, G)\} = \left\{(0,0), (N_C, 0.05), \left(\frac{N_C + N_D}{2}, 0.5\right), (N_D, 0.95), (1,1)\right\} \tag{2.15}$$

The prescribed blade loading source term is the derivative of G with respect to ξ, scaled by the total swirl change across the stage:

$$\frac{\mathrm{d}}{\mathrm{d}m}(rv_\Theta) = \frac{(rv_\Theta)_{out} - (rv_\Theta)_{in}}{L_{chord}} \cdot \frac{\mathrm{d}G}{\mathrm{d}\xi} \tag{2.16}$$

A hybrid loading strategy is employed, where N_C and N_D are varied linearly across the span $\eta \in [0,1]$, producing a fore-loaded distribution at the hub (N_C, N_D) = (0.10, 0.60) and an aft-loaded distribution at the shroud (N_C, N_D) = (0.35, 0.90). This spanwise variation is known to suppress hub corner separation and tip secondary flows simultaneously (Zangeneh & Hawthorne, 1990).

The swirl and meridional velocity at each grid node are recovered from the converged swirl and streamfunction distribution:

$$v_{\Theta(i,j)} = \frac{(rV_\Theta)_{i,j}}{r_{i,j}}, \quad v_m = \frac{\sqrt{(\partial\Psi/\partial\xi)^2 \cdot g_{22} + (\partial\Psi/\partial\eta)^2 \cdot g_{11}}}{\rho \cdot r \cdot J} \tag{2.17}$$

where g_{11}, g_{22} are the metric tensor components and J is the grid Jacobian. The blade wrap angle is integrated along each meridional streamline from the leading edge:

$$f_{i,j} = f_{i_{LE},j} + \int_{m_{LE}}^{m} \frac{(rv_\Theta)/r^2 - \omega}{v_m} \mathrm{d}m' \tag{2.18}$$

During the iterative computation, the thermodynamic closure is achieved by the adiabatic, inviscid-core flow assumption; the specific entropy is held constant at its inlet value $s(\xi, \eta) = s_{in}$ obtained directly from IAPWS-IF97 at the design inlet state (P_0, T_0) of the working fluid; similarly, (ρ, h, T) are evaluated from the IAPWS steam property tables.

The inlet and outlet blade angles are subsequently evaluated from Euler's turbomachinery equation

$$\beta = \arctan\left(\frac{v_m}{u - v_\Theta}\right), \quad u = \omega r \tag{2.19}$$

The iterative process continues until convergence is achieved, with variation in density and wrap angle less than the convergence tolerance. The stage performance coefficients are evaluated at the converged mean radius:

$$\phi = \frac{v_{m,mean}}{u_m}, \quad \lambda = \frac{\Delta h_0}{u_m^2}, \quad \Delta h_0 = \omega\left[(rv_\Theta)_{in} - (rv_\Theta)_{out}\right] \tag{2.20}$$

The algorithm outputs the spanwise inlet and outlet blade angles, wrap angle distribution, and the blade loading curve along the flow streamline. These outputs serve as the direct inputs for the blade profile generation in CFturbo.

Table 1. Thermodynamic and geometric input parameters.

S/N	Parameters	Symbol	Values	Source
1	**Mass Flow Rate**	$\dot{m}$	1.8 kg/s	Prototype testing condition
2	**Inlet Total Temperature & Pressure**	T_o, P_o	150˚C 2.5 bar	Prototype testing condition
3	**Inlet Stagnation Entropy, and Enthalpy**	s, h	7.171 kJ/(kg·K) 2765.2 kJ/kg	IAPWS-IF97 at (T_o, P_o)
4	**Hub and Shroud Diameter**	D_h, D_s	80 mm 240 mm	Geometrically scaled (0.75 scale factor)
5	**Hub-to-shroud Ratio**	D_h/D_s	0.333	Scale-invariant
6	**Blade number**	Z	14	Blade solidity criterion
7	**Degree of Reaction**	R	0.25	Literature
8	**Rotational speed**	$N(\omega)$	4000 rpm (418.9 rad/s)	Flow-coefficient target
9	**Stage Enthalpy drop**	Δh_0	1965 J/kg	Equation (2.20)
10	**Flow coefficient**	φ	1.02	Equation (2.20)
11	**Stage Loading coefficient**	λ	1.75	Equation (2.20)
12	**Discretization Nodes (Streamwise × Spanwise)**	N_{nodes}	1200 (60 × 20)	n_i, n_j
13	**Convergence tolerance**	ε	1×10^{-4}	Wrap angle & Density residual
14	**Loading strategy**	—	Hybrid	Zangeneh Parameterization
15	**Max outer/inner iterations**	—	30, 20	Solver parameters

2.3. CFturbo Inverse Design Implementation

The inverse design flow solver integrates the theoretical aspects with practical generation of blade profiles, utilizing computed parameters such as blade inlet, outlet, and wrap angles, as well as the blade loading distribution from MATLAB, to create 3D blade geometry that meets flow tangency conditions.

The inverse design method implementation in CFturbo consists of five stages that convert theoretical models into geometric, thermodynamic, and aerodynamic constraints, culminating in a blade profile that meets the tangency flow condition. The stages are: main dimension specification, meridional contour definition, blade property assignment, meridional meanline parameterization, and blade profile generation. The hub and shroud diameters, hub-to-shroud ratio, and meridional expansion ratio are specified in the first two stages. The blade number, span positions, and the swirl and wrap angle distributions from MATLAB are assigned in stages three and four, respectively. Blade thickness and camber symmetry distributions are then applied in the final stage to ensure geometric consistency with the design methodology.

2.3.1. The Flow Tangency Condition

The flow tangency condition states that the blade surface must be parallel to or aligned with the local relative velocity field to ensure smooth flow at the boundary layer (blade-fluid contact point).

Mathematically, the unit vector normal to the blade surface must be orthogonal to the velocity field and can be expressed as

$$v \cdot n = 0 \tag{2.21}$$

2.3.2. Iterative Geometry Computation and Convergence

The implementation of the flow tangency condition involves an iterative process within the IDM framework. Convergence refers to the state where successive modifications to the blade wrap angles and geometry fall within a prescribed tolerance. In this work, the iterative loop can be summarized as

- Initialize the blade wrap angle from the meridional meanline specification.
- Compute the relative vector field and evaluate the tangency residuals along the span.
- Update the blade profile to reduce deviations between the velocity vectors and surface normal.
- The processes above are repeated until the residuals fall below the convergence threshold.

The IDM uses iterative procedures to compute an optimal and aerodynamically correct blade profile for the axial flow steam turbine. The inverse design flow solver workflow for the design of the axial flow steam turbine is highlighted in Figure 3.

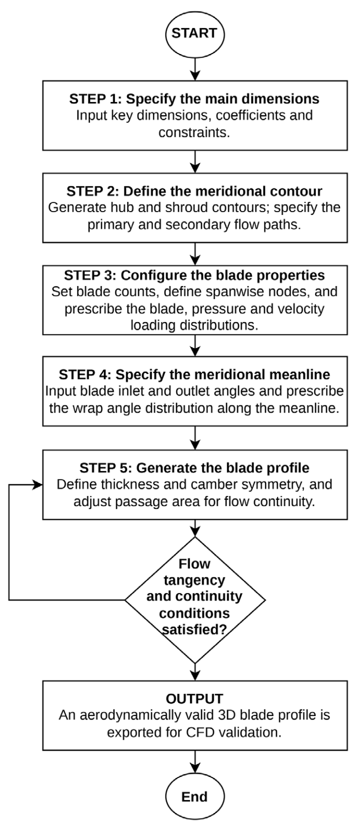

Figure 3. CFturbo inverse design flowchart.

2.4. CFD Validation Framework in ANSYS CFX

The performance of the blade profile generated from the CFturbo inverse design flow solver is validated using steady RANS CFD in the ANSYS CFX simulation environment. This ensures that the blade profiles meet the desired aerodynamic and thermodynamic properties.

The blade profile in STEP format is imported into ANSYS DesignModeler, where the fluid passage is created by Boolean subtraction of the solid blade from an enclosing fluid domain. A cylindrical rotating subdomain is defined around the rotor, and named selections are assigned to the inlet, outlet, blade walls, shroud, and rotating region.

2.4.1. Mesh Generation and Independence Study

A high-quality mesh of the model is crucial to the CFD simulations. Constructs, such as the boundary layers and tip leakages in unshrouded blades, are resolved using the inflation layer in ANSYS Mechanical ADPL. For an accurate representation of flow physics, the following features were implemented during meshing:

1) Local Refinement:

Regions near the leading and trailing edges, suction and pressure sides, and the leakage gaps near the blade tip have higher mesh density and smaller element size due to their high curvatures to capture steep velocities and pressure gradients.

2) Inflation Layers:

For proper flow representation of constructs like boundary layers, the inflation layers are applied along the walls.

3) Mesh Quality and Statistics:

Three systematically refined mesh levels (coarse, medium, and fine) were generated for the rotor domain, with a target refinement ratio of $\sqrt{2}$ between successive levels, following the standard CFD practice (ASME V&V 20). The simulation was deemed mesh-independent once the percentage change in the parameters between the medium and fine levels fell below 5%. The Grid Convergence Index (GCI) was computed to quantify discretization uncertainty. Table 2 presented Mesh Refinement Study Parameters.

Table 2. Mesh refinement study parameters (rotor domain).

Domain	Mesh Level	Element Size (mm)	Nodes Count	Elements Count	Parameter (Outlet Temperature & Pressure)	% Change
Rotor	**Coarse**	20.86	9192	35,178	404.11 K, 1.85 bar	—
	Medium	20.86	17,765	75,386	404.39 K, 1.83 bar	+0.007%, −1.08%
	Fine	45.00	240,651	1,313,105	401.44K, 1.82 bar	−0.66%, −1.62%

Mesh-independence and turbulence-model sensitivity studies were performed on the rotor domain (dominant for blade loading and secondary flows).

2.4.2. Flow Physics Setup

Steam is modeled using real-gas properties derived from the IAPWS-IF97 formulation supported by the ANSYS material library, thus ensuring consistency with the thermodynamic framework employed in the design-stage calculations. The energy equation is enabled in all three domains to capture compressibility effects, temperature variation, and entropy production through the stage.

The SST k-ω (Shear Stress Transport) turbulence model was employed as the primary due to its robustness in predicting boundary layer separation, adverse pressure gradient recovery, secondary flow, and laminar-turbulent transition in turbomachinery cascades (Menter, 1994). A turbulence-model sensitivity study was conducted on the same fine mesh with the k-ε and Spalart-Allmaras model, with model sensitivity assessed by comparing the resulting total-to-total isentropic efficiency, power and torque coefficients, and the total pressure ratios across the three models. A deviation of less than 5% in these parameters relative to the SST k-ω baseline was taken as evidence that the reported results are not strongly mesh- and turbulence-model-dependent.

Total pressure and temperature are specified at the inlet; static pressure is specified at the outlet to enforce the design expansion ratio. No-slip and adiabatic conditions are applied to all solid walls. The rotor domain is treated in the Multiple Reference Frame (MRF) rotating at the design angular velocity ω about the machine axis. Table 3 exemplified Turbulence Sensitivity.

Table 3. Turbulence sensitivity table.

Turbulence model	Total-to-Total Isentropic efficiency η_{tt} %	Power coefficient ($\zeta = \dfrac{Power}{\rho N^3 D^5}$)	Torque coefficient ($\tau = \dfrac{Torque}{\rho N^2 D^5}$)	Total pressure ratio ($\pi = \dfrac{P_{total,out}}{P_{total,in}}$)	Deviation from baseline (SST) %
SST k-ω	16.38	0.11	3.12	0.891	-
k-ε	52.827	0.15	4.39	0.849	<5% (for π and flow angles)
Spalart-Allmaras	52.897	0.15	4.42	0.847	<5% (for π and flow angles)

2.4.3. Postprocessing and Validation Metrics

The CFD simulation results were analyzed and processed to extract meaningful and actionable insights. Visual inspection of the flow field streamlines along the blade surface and within the blade passages is crucial for identifying regions of high pressure or velocity gradients, flow separation, leakage vortices, and other undesirable flow phenomena.

Furthermore, the stage efficiency, density, pressure, temperature, mass flow rate, and output work are quantified and compared with predictions from the classical Euler turbine equations as a cross-validation technique. The accuracy and effectiveness of the inverse design methodology were verified using computational fluid dynamics (CFD) simulations in ANSYS CFX, following the workflow presented in Figure 4.

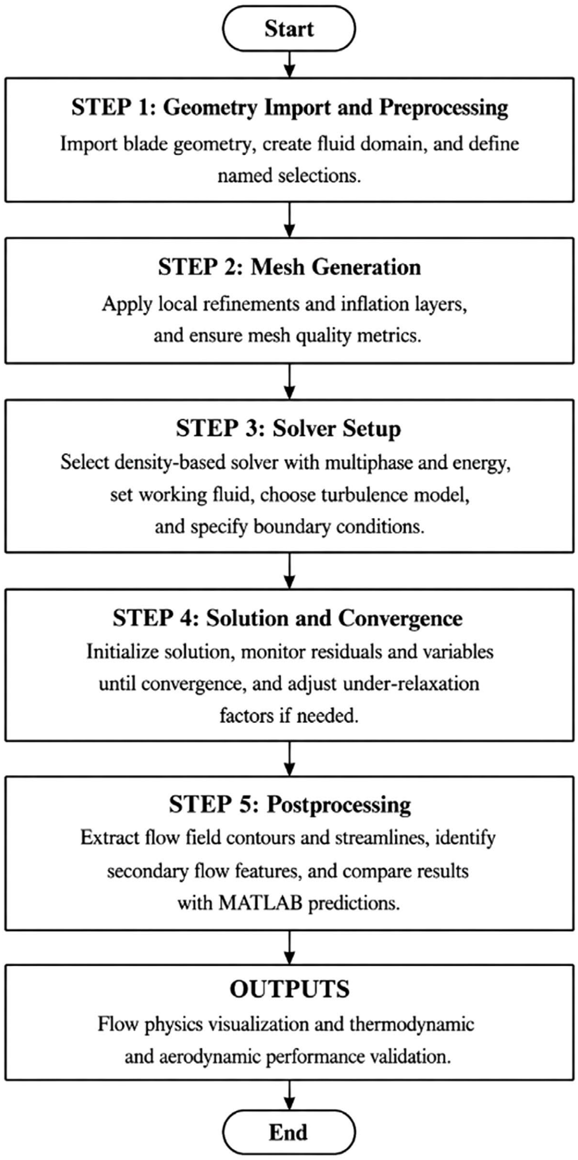

Figure 4. ANSYS CFX simulation workflow for the CFD validation.

2.5. Prototype Development and Material Considerations

The final step of the methodology adopted for this study is the design and development of the prototype. A geometrically scaled prototype of the designed blade geometry is fabricated by fused deposition modeling (FDM), selected for its suitability in reproducing the intricate curvature of inverse-designed turbomachinery blades. The prototype geometry (D_h = 60 mm, D_s = 180 mm) was obtained by uniform geometric scaling (factor k = 0.75) of the design-scale blade profile (D_h = 80 mm, D_s = 240 mm), preserving all non-dimensional flow parameters.

The prototype material is a high-strength polymer resin offering a practical balance between dimensional fidelity and printability. The prototype serves as a proof-of-concept demonstration of the IDM workflow's compatibility with additive manufacturing rather than as a performance measurement platform.

2.6. Design Calculations

The baseline parameters of the steam turbine, such as the stage loading and flow coefficients, hub and shroud dimensions, meanline span, blade solidity, and the number of blades, which are critical for defining the initial geometry and the operational constraints of the turbine, are specified in this section.

2.6.1. Hub-to-Shroud Ratio and the Meanline Span

The hub-to-shroud ratio $\frac{D_h}{D_s}$, governs spanwise flow distribution and structural design. For the present design-scale geometry ($D_h = 80\ \text{mm}$, $D_s = 240\ \text{mm}$):

$$\frac{D_h}{D_s} = 0.333,\ \ B = \frac{D_s - D_h}{2} = 80\ \text{mm}.$$

This ratio is preserved under geometric scaling for prototype fabrication (Section 2.5) since it is scale-invariant. The value 0.333 falls marginally below the typical range for reaction turbines, which is acceptable given the low degree of reaction ($R = 0.25$), shifting the design toward the impulse regime.

2.6.2. The Blade Solidity and the Number of Blades

The blade solidity, σ is defined as the ratio of the chord length to pitch, with a typical range $\sigma \in [0.7, 1.1]$ at the midspan (Douglas, 2005). This value directly computes the required number of blades, Z, of the steam turbine.

$$\sigma = \frac{c}{s},\ \ Z = \frac{\pi D_m}{s} \tag{2.22}$$

2.6.3. The Stage Loading and Flow Coefficients

The non-dimensional stage loading coefficients λ, and flow coefficients ϕ, provide the performance parameters in steam turbine design and are defined as:

$$\psi = \frac{\Delta h_o}{u^2},\ \ \phi = \frac{V_m}{u} \tag{2.23}$$

Literature suggests $\lambda \in [1.5, 2.0]$ and $\phi \in [0.5, 0.7]$ for the axial steam turbines (Douglas, 2005). For the present design, $\lambda = 1.75$ falls centrally within range. The flow coefficient $\varphi = 1.02$ lies slightly above the typical band. This results from the prescribed mass flow rate and inlet conditions fixing meridional velocity via continuity, with rotational speed (4,000 rpm) chosen for practical operation; such trade-offs are common in small-scale, low-density steam turbines.

3. Results and Discussion

This chapter presents the results of the inverse design method (IDM) implementation for the single-stage axial steam turbine, including ANSYS CFX simulation, validation, and prototype testing, presented in the sequence of the design workflow: MATLAB numerical solution, CFturbo blade geometry generation, and CFD validation.

A consolidated quantitative comparison across all three stages (Table 2) is presented in Section 3.5, providing the numerical basis for the cross-method agreement claims stated in the Abstract.

3.1. MATLAB Implementation Results

The MATLAB solver converged to a spanwise blade angle distribution across nine radial stations from hub to shroud within the outer-loop tolerance ε. Inlet blade angles ranged from 70˚ to 150˚ and outlet blade angles from 20˚ to 55˚, both consistent with published design envelopes for single-stage axial steam turbines (Dixon & Hall, 2014). The spanwise angle distributions are presented in Figure 5 alongside the corresponding CFturbo evaluation.

The hybrid loading strategy produced a fore-loaded profile at the hub (peak of $dG/d\xi$ near $\xi \approx 0.3$) and an aft-loaded profile at the shroud (peak near $\xi \approx 0.7$), with a smooth monotone transition across the span at intermediate η values. The blade wrap angle varied monotonically along the meridional chord at each spanwise section, confirming both the feasibility of the prescribed loading function and the numerical stability of the solver. The resulting blade loading curve along the meridional length is presented in Figure 5.

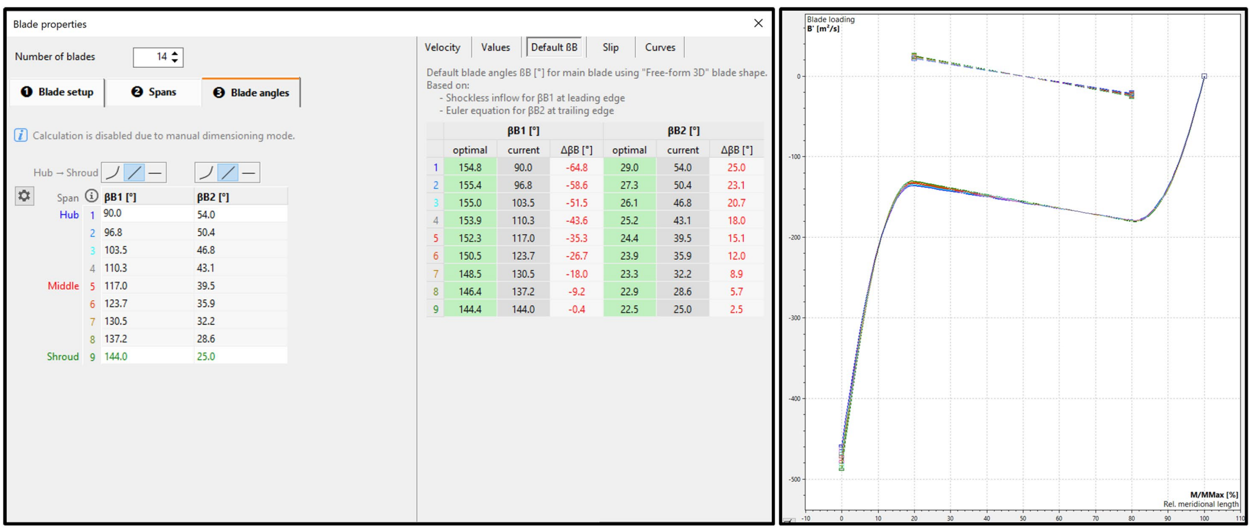

Figure 5. Spanwise blade angle and loading distribution.

3.2. CFturbo Implementation of the Inverse Design Methodology

The geometric profile of the blade was generated using the inverse design flow solver from the MATLAB-computed distributions. The CFturbo IDM solver generated blade geometry for the inlet stator, rotor, and outlet stator (Figure 6(A), Figure 6(B)) from the MATLAB-computed angle distributions and prescribed swirl profile. All three blade surfaces exhibit smooth camber and a continuous variation in thickness from hub to shroud, confirming effective enforcement of the flow tangency condition throughout the iterative geometry computation. Table 4 presented the Thermodynamic Parameters Derived from CFturbo Implementation.

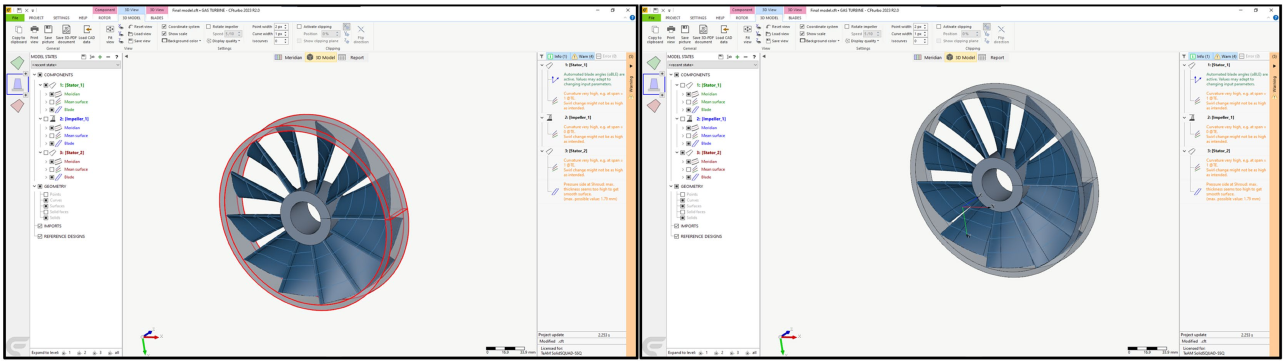

(A)

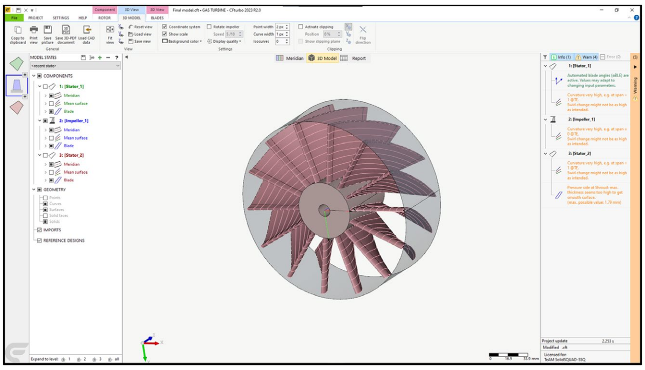

(B)

Figure 6. (A) Blade geometry generated in CFturbo for the inlet and outlet stator; (B) Blade geometry generated in CFturbo for the rotor.

Table 4. Thermodynamic parameters derived from CFturbo implementation.

S/N	Parameters	Symbols	Values
1	Hub-to-shroud diameter ratio	D_h/D_s	0.333
2	Isentropic to static velocity ratio	u/c_0	0.352
3	Isentropic to static efficiency ratio	η_{ts}	0.707
4	Temperature ratio	T_2/T_1	0.811
5	Density ratio	ρ_2/ρ_1	0.843
6	Pressure ratio	P_2/P_1	0.677
7	Absolute Mach number	Ma	0.611
8	Specific diameter (Balje)	δ	1.796

3.3. CFD Validation Results

The inverse-designed blade profile generated in the flow solver was validated using computational fluid dynamics in ANSYS CFX. The flow-blade interaction and flow phenomena such as turbulence, energy and momentum transport, and the flow convergence behavior were studied in this section.

3.3.1. Computational Domain and Flow Field Visualization

The computational domain comprising the blade, rotating frame, and fluid region, imported and modified in the ANSYS DesignModeler environment, was meshed and solved using the ANSYS CFX solvers as a coupled system under identical boundary conditions.

The flow field visualization from the CFX result confirmed a smooth flow of the working fluid over the blade profile.

3.3.2. The Flow Streamlines, Pressure, Velocity, and Temperature Contours

The flow streamlines, static pressure, velocity, and temperature contours along the meridional axis and flow passage depict regions of mass, momentum, and energy transfer and the overall thermal and aerodynamic properties of the steam turbine.

The figures below depict the streamline, pressure, and velocity gradients along the steam turbine.

3.3.3. Blade Loading Distribution

The computed blade loading distribution from the CFD results showed excellent consistency with the mid-loaded pattern prescribed in the MATLAB computation, with peak loading and circulation at mid-span and reduced turning at the hub and shroud regions.

3.4. Discussion

The inverse design methodology implemented in this study demonstrated strong consistency between the analytical, numerical, and CFD-based predictions of the turbine flow field. The spanwise blade angles, loading distribution, and wrap angle obtained from MATLAB were validated against CFturbo's inverse design solver, showing a strong correlation, which confirms the reliability of the derived quasi-3D formulation.

The flow visualization in ANSYS CFX revealed smooth streamlines along both stator and rotor passages, indicating effective control of flow turning and suppression of separation zones, phenomena typically associated with forward-designed blades. Pressure contours across the rotor passage displayed a steady pressure gradient from leading to trailing edges, confirming an efficient energy exchange between steam and blades. The mid-loaded circulation pattern predicted numerically was preserved in the CFD results, reinforcing that the prescribed loading function led to a balanced aerodynamic configuration.

Velocity and temperature contours also showed good agreement with theoretical expectations, demonstrating gradual velocity recovery downstream and minimal wake distortion. The low Mach numbers throughout the passage confirmed that the model accurately captured compressibility effects, while entropy gradients remained within stable limits, validating the inclusion of compressibility correction in the quasi-3D formulation.

Overall, the combined results verify that the inverse design methodology can effectively produce physically consistent and aerodynamically smooth blade geometries for steam turbine applications. The agreement between MATLAB predictions, CFturbo geometries, and CFD simulations establishes IDM as a robust and practical design tool capable of bridging theoretical derivation and industrial implementation.

3.5. Summary

This chapter presented and discussed the results obtained from the inverse design methodology implemented in MATLAB and CFturbo and the validation using the ANSYS simulation environment. The outcomes confirmed the superiority of the inverse design method over the traditional direct design approach in achieving the desired flow and energy conversion efficiency (see Figure 7).

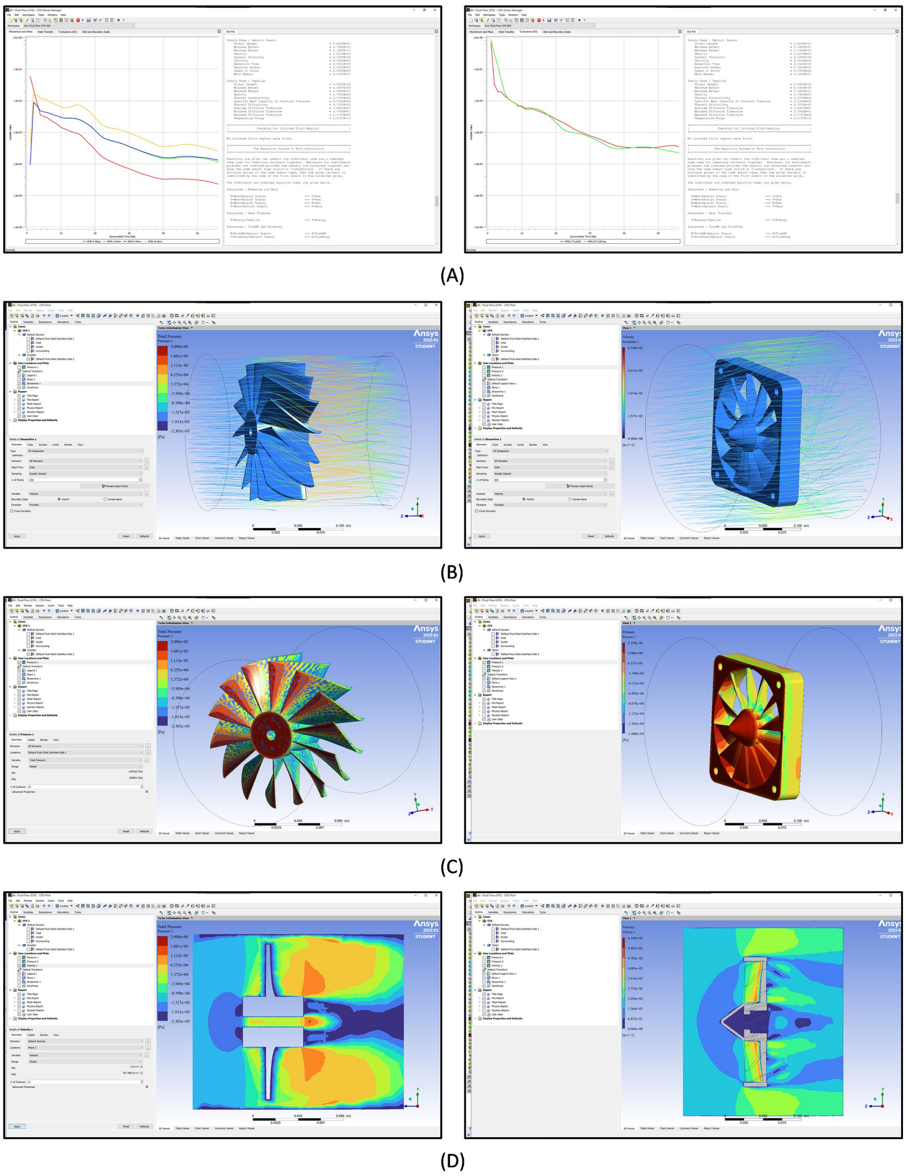

Figure 7. (A) Mass, momentum, and turbulence convergence plots; (B) Streamline flow visualisation along the rotor and inlet stator passage; (C) Pressure contour along the rotor and inlet stator; (D) Velocity contour visualisation along the rotor and inlet stator.

4. Conclusions

4.1. Overview

This chapter summarizes the key findings from the design and development of a single-stage axial flow steam turbine using the inverse design methodology. The research successfully demonstrated the mathematical rigor, computational implementation, and practical feasibility of the IDM approach for steam turbine blade design.

The chapter presents the main conclusions drawn from the study, evaluates the achievement of research objectives, discusses the contributions to knowledge, identifies limitations, and provides recommendations for future research.

4.2. Key Findings

A quasi-3D streamfunction-vorticity formulation was derived from the compressible Navier-Stokes equations to capture the essential flow physics of steam with entropy effects. The numerical implementation in MATLAB yielded blade angles, wrap angle, and blade loading distributions consistent with published data for axial turbines.

The subsequent integration with CFturbo's IDM module enabled direct translation of the computed aerodynamic parameters into a three-dimensional blade geometry that satisfies the flow tangency condition. CFD validation in ANSYS CFX confirmed the predicted aerodynamic performance, showing uniform pressure and velocity fields and minimal secondary flow formation. These results demonstrate that the adopted IDM framework provides a more efficient and physically intuitive approach to blade design than the conventional forward design method.

4.3. Significance and Contributions to Knowledge

1) The study demonstrates that the inverse design methodology is a practical and rigorous alternative to conventional steam turbine design approaches, with the main contributions summarized as follows: Theoretical Advancement: Extension of the quasi-3D inverse design framework to compressible flow with entropy-gradient terms, enabling more realistic modeling of steam expansion.

2) Methodological Contribution: Establishment of a reproducible workflow linking analytical computation (MATLAB), inverse design software (CFturbo), and CFD verification (ANSYS CFX).

3) Computational Efficiency: Reduction of iterative optimization cycles by directly prescribing desired flow behavior, improving design accuracy with fewer computational resources.

4) Practical Relevance: Demonstration of compatibility between academic modeling and commercial design platforms, supporting future industrial applications of IDM-based turbine design.

4.4. Limitations and Future Works

Although the developed framework proved robust, certain simplifications were necessary. The current formulation neglects viscous dissipation within the blade boundary layer and relies on meanline approximations for radial variations. The CFD validation, while comprehensive, was limited to steady-state simulations without experimental correlation.

Future studies in this field should address the following:

- Extend the governing equations to fully 3-D viscous formulations and transient CFD models.
- Incorporate loss correlations and turbulence-entropy coupling for improved thermodynamic prediction.
- Perform experimental validation through prototype or cascade-test measurements to establish empirical accuracy.

4.5. Final Remarks

The implementation of the quasi-3D inverse design method to steam-turbine blade design in this study has proven to be both mathematically rigorous and computationally feasible. The integration of analytical derivation, numerical implementation, and CFD validation demonstrates a complete and reliable framework for high-efficiency turbomachinery design.

By directly linking desired aerodynamic behavior to resulting blade geometry, IDM provides a decisive step toward faster, more accurate, and physically consistent turbine design methodologies. This work therefore contributes a significant academic and practical foundation for future studies and industrial adoption of flow-driven design principles in steam-turbine development.

Acknowledgements

The authors acknowledge the supportive academic environment and resources provided by the Department of Mechanical Engineering, Obafemi Awolowo University (OAU), which facilitated effective collaboration and mentorship throughout this work. The authors appreciated and also acknowledged the computational support of the Cybersecurity Laboratory of the African Centre of Excellence (ACE) under the World Bank Project Grant No: P169064 at the Obafemi Awolowo University, Ile-Ife, Nigeria.

Authors' Contributions

Ayodele T. Oyeniran: original concept, supervision, review and editing; Olamilekan Agbedun: editing and writing; Ayomide E. Oyedare: reviewed existing models, new model development, model validation, editing and writing; Daniel S. Taiwo: review, editing and writing; Samson K. Fasogbon: review, editing and writing; Opeyemi B. Daniyan: review, editing and writing; Abraham A. Asere: review, editing and writing.

Conflicts of Interest

The authors declare no known conflict of interest.

References

[1] Ramabose, K. and Ganesan, S. (2019) A Study on Household Sector Energy Consumption of Rural and Urban Areas in Virudhunagar District of Tamil Nadu. *Shanlax International Journal of Economics*, **8**, 21-31. https://doi.org/10.34293/economics.v8i1.902

[2] Meher-Homji, C.B. (2000) The Historical Evolution of Turbomachinery. Texas A&M University.

[3] Dixon, S.L. and Hall, C.A. (2014) Fluid Mechanics and Thermodynamics of Turbomachinery. 7th Edition, Butterworth-Heinemann.

[4] Nag, P.K. (2008) Power Plant Engineering. Tata McGraw-Hill Education.

[5] Denton, J.D. (1993) The 1993 IGTI Scholar Lecture: Loss Mechanisms in Turbomachines. *Journal of Turbomachinery*, **115**, 621-656. https://doi.org/10.1115/1.2929299

[6] Giuffre, A. and Pini, M. (2020) Design Guidelines for Axial Turbines Operating with Non-Ideal Compressible Flows. *Journal of Engineering for Gas Turbines and Power*, **143**, Article ID: 011004. https://doi.org/10.1115/1.4049137

[7] Gribin, V., Tishchenko, A., Gavrilov, I., Tishchenko, V., Sorokin, I. and Alexeev, R. (2017) Turbine Blade Profile Design Method Using Bezier Curves. *European Conference on Turbomachinery Fluid Dynamics and Thermodynamics*, Stockholm, 3-7 April 2017. https://doi.org/10.29008/etc2017-195

[8] Hosseini, S.A., Nakisa, M. and Lakzian, E. (2023) Reducing the Condensing Flow Effects on the Steam Turbine Blades through Modified Design Geometry. *Physics of Fluids*, **35**, Article ID: 095119. https://doi.org/10.1063/5.0166144

[9] Boselli, P. (2016) An Inverse Design Methodology for Long Last-Stage Steam Turbine Blades. Doctoral Thesis, University College London.

[10] Rajendran, N., Prasad, B. and Sanyasiraju, Y.V.S.S. (2017). Development of Turbine Blade Profiles Using Iterative Inverse Design Methodology. *Proceedings of the ASME* 2017 *Gas Turbine India Conference*, Bangalore, 7-8 December 2017, V001T02A003. https://doi.org/10.1115/gtindia2017-4553

[11] Zanetti, G., Siviero, M., Cavazzini, G. and Santolin, A. (2023) Application of the 3D Inverse Design Method in Reversible Pump Turbines and Francis Turbines. *Water*, **15**, Article No. 2271. https://doi.org/10.3390/w15122271

[12] Zhou, H., Yu, K., Luo, Q., Luo, L., Du, W. and Wang, S. (2022) Design Methods and Strategies for Forward and Inverse Problems of Turbine Blades Based on Machine Learning. *Journal of Thermal Science*, **31**, 82-95. https://doi.org/10.1007/s11630-022-1544-6

[13] Zangeneh, M. and Hawthrone, W.R. (1990). A Fully Compressible Three Dimensional Inverse Design Method Applicable to Radial and Mixed Flow Turbomachines. *ASME* 1990 *International Gas Turbine and Aeroengine Congress and Exposition*, Brussels, 11-14 June 1990, V001T01A059. https://doi.org/10.1115/90-gt-198

[14] Smith, J. (2020) Modeling and Simulation of Fluid Dynamics in Turbomachinery. *American Journal of Mechanical Engineering and Technology*, **1**, 1-10. https://doi.org/10.71465/ajmet1988

[15] Rahmati, M.T. (2009) Inverse Approach to Turbomachinery Blade Design. *AIAA Journal*, **47**, 703-709. https://doi.org/10.2514/1.38856

[16] Douglas, J.F., Gasiorek, J.M., Swaffield, J.A. and Jack, L.B. (2005) Fluid Mechanics. 5th Edition, Ashford Colour Press Ltd.

Nomenclature

a	Speed of sound [m/s]
B	Blade height/span [m]
D_h, D_s	Hub, Shroud diameter [m]
f, β	Blade wrap angle [rad], Relative flow angle [˚]
g_{11}, g_{22} & J	Metric tensor components, Grid Jacobian
h, s	Specific enthalpy [J/kg·K], specific entropy [J/kg·K]
L_m, m	Meanline length, meridional coordinate
$\dot{m}$	Mass flow rate [Kg/s]
N, ω	Rotational speed [rpm], angular velocity [rad/s]
P, T	Static pressure [Pa], temperature [K]
r, z, θ	Cylindrical coordinates
R	Degree of reaction
u	Blade peripheral speed [m/s]
Z	Number of blades
ε	Convergence tolerance
ρ, v	Density [kg/m^3], specific volume [m^3/kg]
ω_θ, σ	Circumferential vorticity, Blade solidity
φ, λ	Flow coefficient; stage loading coefficient
Γ, ψ	Circulation around blade [m^2/s], Streamfunction [m^2/s]